





Cite this: *RSC Adv.*, 2021, 11, 36801

# A V(III)-induced metallogel with solvent stimuli-responsive properties: structural proof-of-concept with MD simulations†

Sima Sedghiniya,<sup>a</sup> Janet Soleimannejad,<sup>a</sup> <sup>\*,a</sup> Masumeh Foroutan,<sup>\*,a</sup> Mina Ebrahimi <sup>a</sup> and Vahid Fadaei Naeini <sup>b</sup>

A new solvent stimuli-responsive metallogel (VGel) was synthesized through the introduction of vanadium ions into an adenine (Ade) and 1,3,5-benzene tricarboxylic acid (BTC) organogel, and its supramolecular self-assembly was investigated from a computational viewpoint. A relationship between the synthesized VGel integrity and the self-assembly of its components is demonstrated by a broad range of molecular dynamics (MD) simulations, an aspect that has not yet been explored for such a complex metallogel in particular. MD simulations and Voronoi tessellation assessments, both in agreement with experimental data, confirm the gel formation. Based on excellent water stability and the ethanol/methanol stimuli-responsive feature of the VGel an easy-to-use visualization assay for the detection of counterfeit liquor with a 6% (v/v) methanol limit of detection in 40% (v/v) ethanol is reported. These observations provide a cheap and technically simple method and are a step towards the immersible screening of similar molecules in methanol-spiked beverages.

Received 20th September 2021

Accepted 9th November 2021

DOI: 10.1039/d1ra07055j

rsc.li/rsc-advances

## 1. Introduction

On-the-spot detection of alcohol content and methanol-containing counterfeit beverages is a serious challenge. Methanol poisoning is attributed to its metabolism into toxic formic acid and formaldehyde and causes serious eye and nervous system damage, or even death.<sup>1–3</sup> Especially in developing countries such as Iran and India, methanol poisoning outbreaks have happened recently and during the coronavirus pandemic with hundreds of victims due to counterfeit drinking products. Drinking as little as 240 ml of 12.5% (v/v) of methanol can be fatal,<sup>4</sup> and also the US<sup>5</sup> and EU<sup>6</sup> safety threshold for methanol in liquor (40% (v/v) ethanol) is 0.4% (v/v). With this in mind, a methanol detector for screening in the toxic range could serve a major cause and help prevent methanol poisoning outbreaks. While some methods such as near-infrared assays,<sup>7–10</sup> Raman spectroscopy,<sup>9–11</sup> enzymatic methods,<sup>12–14</sup> and chromatography,<sup>2,15–21</sup> have been used to figure out alcohol content and detect methanol-spiked liquor, most of the methods are expensive and rarely accessible<sup>9–11,14,21</sup> in developing countries where the majority of methanol poisoning outbreaks happen.

To relieve these restrictions, different compounds ranging from nanomaterials to supramolecular polymers with this perspective, have been demonstrated<sup>22–26</sup> though the use of gels and metal-organic framework-based materials is very limited.<sup>27–30</sup> Self-assembly of low molecular weight gelators (LMWGs) has led to a series of soft materials in the area of drug delivery systems, tissue engineering scaffolds, cosmetics, indicators, and sensors.<sup>31–34</sup> To bring out the potency of these soft materials in definitive manners for specific applications, tuning of multiple non-covalent interactions such as hydrogen bonding,  $\pi$ - $\pi$  stacking, electrostatic effects, and van der Waals forces, can be helpful.<sup>35–39</sup>

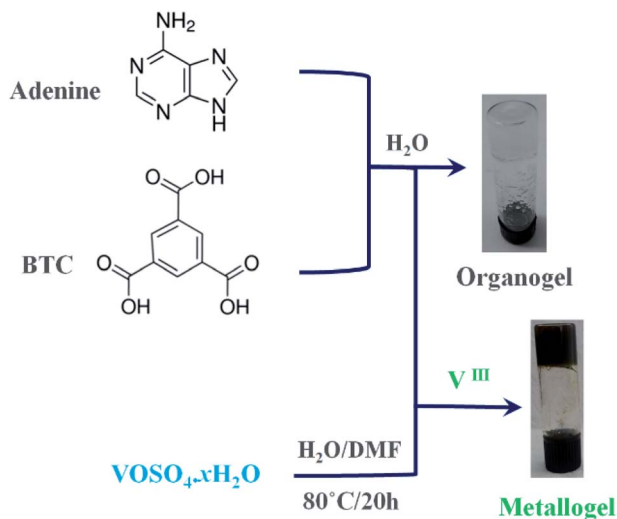
In recent years metallogels have drawn attention, due to their broad range of applications.<sup>36,40–42</sup> In comparison with organogels, in metallogels, the introduction of metal ions into the gelator molecules triggers some of the most fascinating “smart” material features.<sup>43,44</sup> Less-studied metallogels not only merge incorporated metal characteristics (including conductive, catalytic, redox, or optical features) but also introduce additional subtle non-covalent interactions into the resulted molecular assemblies.<sup>44,45</sup> Gel network modifications by appropriate metal ion incorporation can constrain metal interactions and suggesting potent metallogels for visual molecular recognition.<sup>46</sup> The presence of optical and redox-active metal centers is a new platform that was reported for Cu(I) containing metallogels with redox-responsive behavior.<sup>39,47</sup> Other reports in this fascinating research field of metallogels are very rare which leaves an exploratory scope in the case of designing metallogels with redox/optical-switchable behavior.<sup>48–50</sup> Herein we report

<sup>a</sup>School of Chemistry, College of Science, University of Tehran, Tehran, Iran. E-mail: janet\_soleimannejad@khayam.ut.ac.ir; foroutan@khayam.ut.ac.ir

<sup>b</sup>Division of Machine Elements, Luleå University of Technology, Luleå, SE-97187, Sweden

† Electronic supplementary information (ESI) available. See DOI: 10.1039/d1ra07055j





Scheme 1 Vanadium ion entrapment and formation of the VGel metallogel.

the formation of a new metallogel of adenine and 1,3,5-benzene tricarboxylic acid gelators by vanadium metal ion incorporation in the presence of water and DMF solvents.

To assess the rational design along with the parameters that influence the assembly of the gels, it is essential to elucidate the self-assembling mechanism. Molecular dynamics (MD) simulations are ideally suited to probe the self-assembly. To the best of our knowledge, although the self-assembling organization or mechanism of organogels has been extensively explored,<sup>51–54</sup> no detailed investigations of metallogels are available. In this study with MD simulations, the vital roles and the ratio of the

participated solvents ( $\text{H}_2\text{O/DMF}$ ) as well as the other metallogel components are elucidated.

Our metallogel has shown unique ethanol/methanol detection capability which can be used effectively as a metallogel-based indicator. We believe that this differentiating behavior is driven by  $\text{V}^{\text{III}}$  to  $\text{V}^{\text{V}}$  oxidation.

## 2. Materials and methods

### 2.1. Reagents and chemicals

$\text{VOSO}_4 \cdot x\text{H}_2\text{O}$ , 1,3,5-benzene tricarboxylic acid (BTC), adenine, DMF, ethanol ( $\geq 99.5\%$ ) and, methanol (99.8%) were purchased from Sigma-Aldrich and used as supplied. All aqueous solutions were prepared with deionized water.

### 2.2. Synthesis

An aqueous solution of adenine/BTC (4 ml; 0.1/0.12 mmol) was mixed with an aqueous/dimethylformamide ( $v/v = 1/2$ ; 3 ml) solution of vanadyl sulfate (0.1 mmol), negligible green precipitation was formed almost immediately that turned into a dark green (seaweed) opaque metallogel upon heating at 80 °C for 20 hours. In the preparation process, heating temperature, time, cooling rate, and gel components, were evaluated as effective factors, and the optimum conditions were concluded [see pages 3 and 5 in the ESI†].

### 2.3. Apparatus

FT-IR spectra were recorded on a Bruker Tensor 27 spectrometer in the range 500–4000  $\text{cm}^{-1}$  using KBr pellets. UV-visible absorptions were measured at room temperature (23 °C) using a PerkinElmer Lambda 850 spectrometer in the range 800–

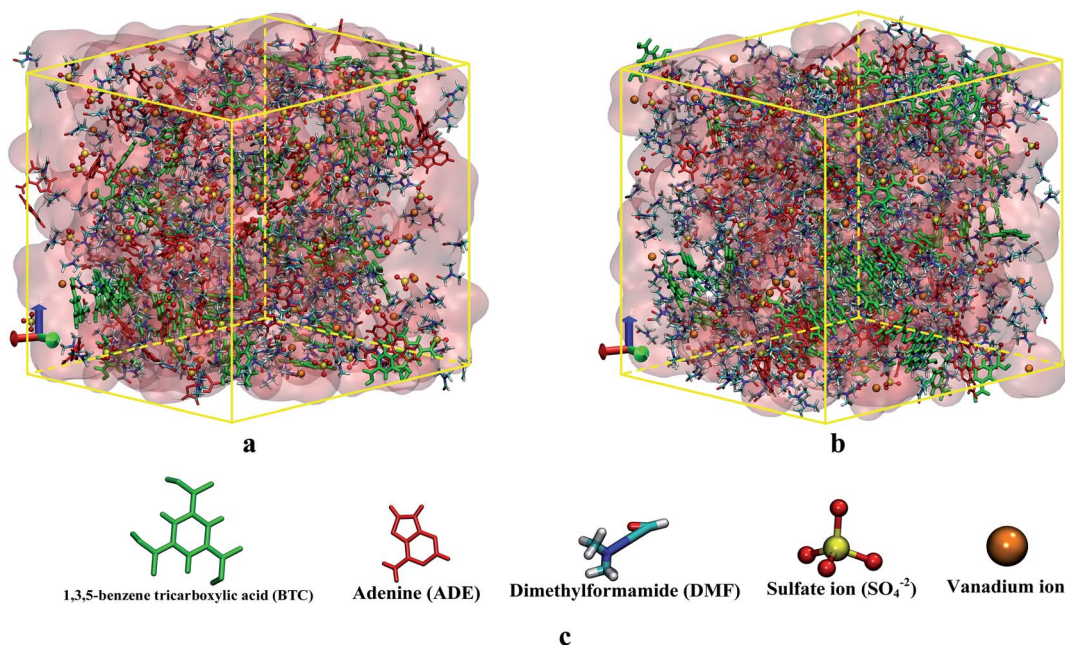


Fig. 1 The MG3 system in the initial (a) and final (b) configurations (water is shown in quick surface representation). (c) VGel components including BTC, Ade, DMF molecules,  $\text{V}^{3+}$  and sulfate ions.



300 nm. Rheological testing of the metallogel was conducted on an Anton Paar, Physica, MCR 300 rheometer, with a 15 mm diameter cone plate.

#### 2.4. Computational details

MD simulations were performed using the NAMD software with a 1 fs time step.<sup>55</sup> For H<sub>2</sub>O, DMF, BTC, adenine, and sulfate ion (SO<sub>4</sub><sup>2-</sup>), the CHARMM36 force field parameters<sup>56,57</sup> were utilized. Lennard-Jones parameters for V<sup>III</sup> and SO<sub>4</sub><sup>2-</sup> ions and their partial charges were taken from the previous works and are presented in Table S1.<sup>†</sup><sup>58–60</sup> The TIP3P water model<sup>61</sup> was applied for each simulation. The simulation of metallogel was carried out in the NPT ensemble (at  $P = 1$  bar), and the pressure was controlled by the Langevin piston extendible along each axis with a decay period of 200 fs. The temperature was controlled by the Langevin thermostat and 5 ps<sup>-1</sup> damping coefficient. Periodic boundary conditions were employed in all directions. Electrostatic interactions were calculated using the particle mesh Ewald (PME) method over a cubic grid with  $\sim 1$  Å spacing,<sup>62</sup> and a 10–12 Å cutoff was implemented for van der Waals (vdW) interactions. The visualization of all simulations was performed with the VMD software 1.9.3 (ref. 63) (for more details see pages 4 and 5 in the ESI<sup>†</sup>).

### 3. Results and discussion

#### 3.1. Rationale and design of the VGel

Among the nucleobase ligands, guanine-based metallogels with small alkali metals, such as Na<sup>+</sup> and K<sup>+</sup> have been well-documented.<sup>64</sup> In comparison, the chemistry of adenine-based metallogels has been explored very little in this field. The knowledge obtained from the studies on adenine organogels<sup>65–67</sup> and calculations of the interactions between adenine and other components,<sup>68</sup> provides a valuable insight into the design and preparation of a novel adenine-based metallogel with stimuli-responsive features.<sup>69</sup> In our case, the most challenging feature of introducing metal ions into the gel network is the addition of several metal–solvent or metal–ligand interactions, that most probably trigger gel network destruction. Based

on the crystal engineering concepts and proven templating effects of some molecules, the DMF solvent, as the most suitable and accessible template, was selected and examined (Scheme 1).<sup>70</sup>

#### 3.2. Structure–mechanical properties assessment using MD

Three systems (with 71.43 : 28.57, 50 : 50 and, 28.57 : 71.43 v/v% of H<sub>2</sub>O/DMF denoted as MG1, MG2 and, MG3) were simulated and the results have been compared from a gel formation point of view (for more information please see ESI<sup>†</sup>). The self-assembly and structural features accompanying the dynamics and mechanical properties have been studied through the calculation of the non-covalent interactions and simulated shear stress loading, respectively. In Fig. 1, the initial and final configurations of the MG3 system are demonstrated (for MG1 and MG2 systems' snapshots please see Fig. S1<sup>†</sup>).

For structural assessments of the VGel, the radial distribution function (RDF) of V<sup>III</sup> ions concerning each other as well as different solvent ratios (H<sub>2</sub>O/DMF) are inspected (Fig. 2). In the MG3 system, where the metallogel is formed more properly than the MG1 and MG2 systems, the concentration of DMF in the first and neighboring marginal layers of the V<sup>III</sup> ions, is

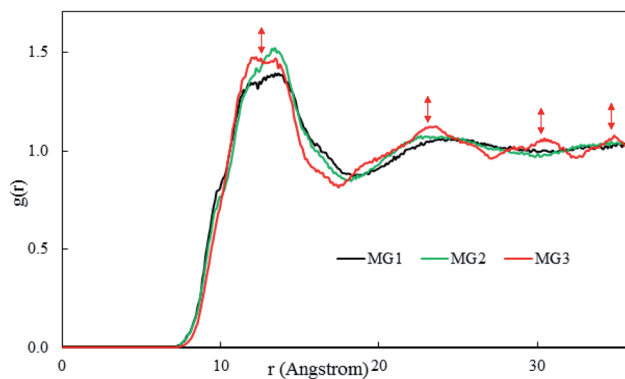


Fig. 3 RDFs between V<sup>III</sup> ions in MG1, MG2, and MG3 systems at room temperature.

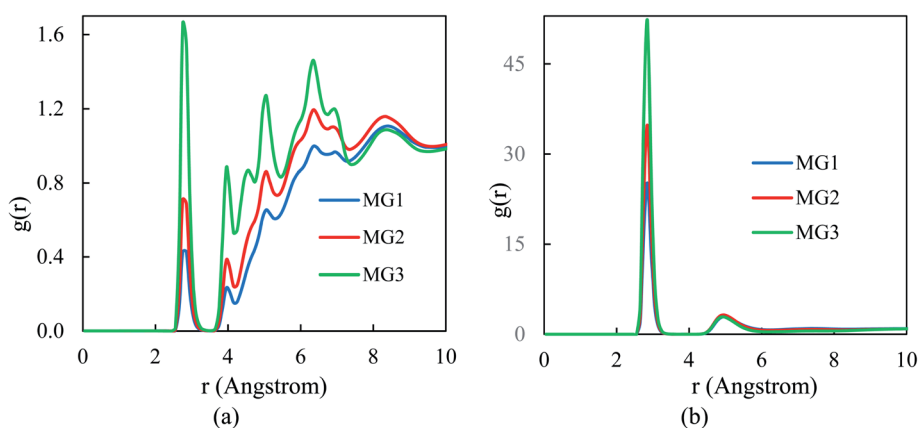


Fig. 2 RDFs between V<sup>III</sup> ions and solvents at room temperature, in MG1, MG2 and MG3 systems. Pair correlation between V<sup>III</sup> ions with (a) DMF and (b) water molecules.

higher (Fig. 2a), and the H<sub>2</sub>O molecules surrounding the V<sup>III</sup> ions are located in a more compact form (Fig. 2b), which makes the nearest neighboring vanadium ions detectable.

In the feeble network of the MG1 and MG2 systems, although the number of water molecules in the first coordination shell of

metal ions is reduced, there is not a remarkable distinction between the densities in the second shell. Generally, Fig. 2a demonstrates large distance surrounding and determinant role of the DMF solvent toward the metallogel formation.

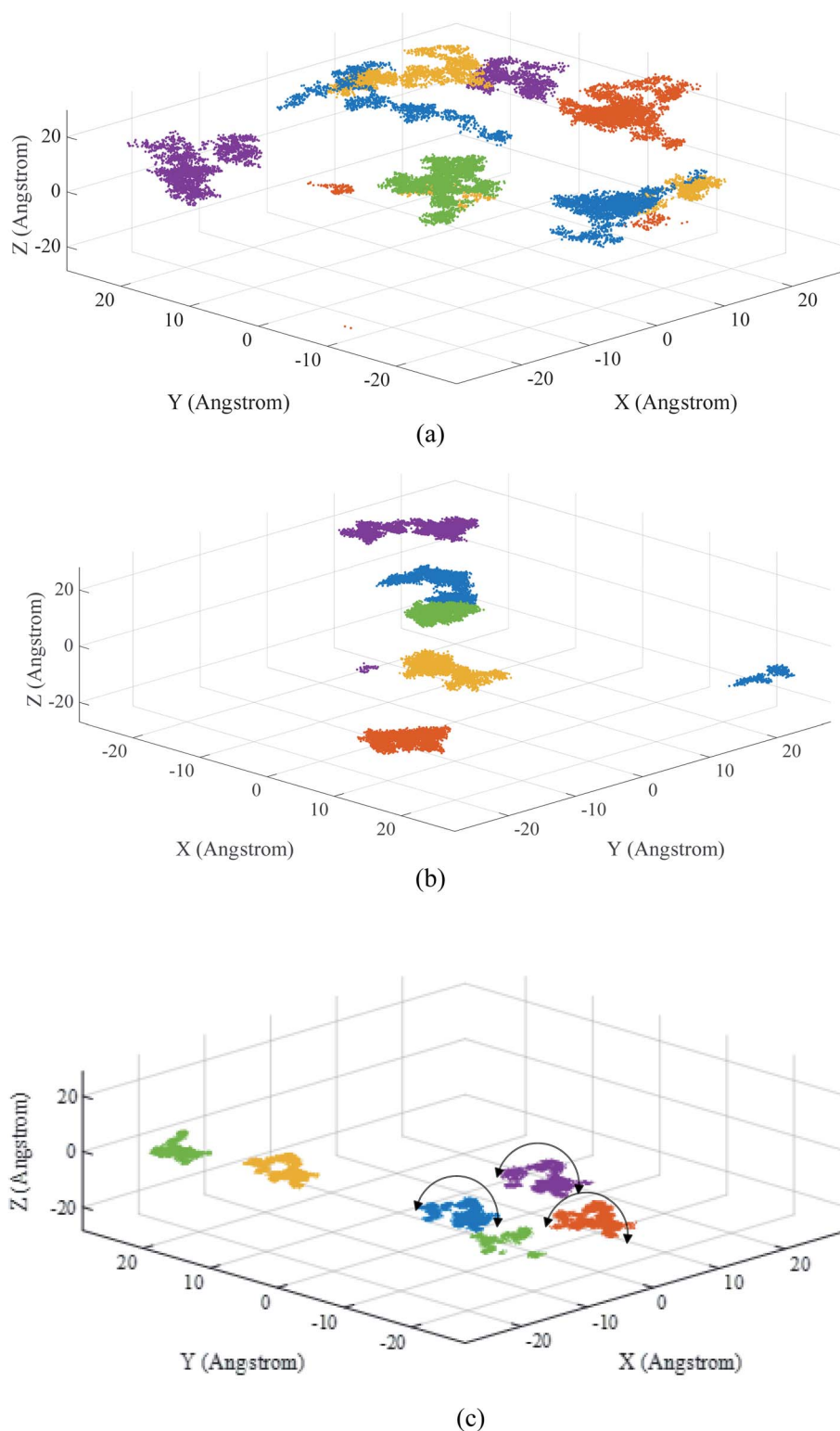


Fig. 4 The 3D trajectories of the marked V<sup>III</sup> ions in the (a) MG1, (b) MG2 and (c) MG3 systems under ambient conditions.



As illustrated in Fig. 3, the RDF of vanadium ions represents relatively higher peaks at 13, 23, 30, and 35 Å and shallower valleys for the MG3 system than the other two systems. It can be inferred from Fig. 3 that by increasing the DMF/H<sub>2</sub>O solvent ratio, the vanadium ions are arranged in a relatively more ordered fashion relative to each other. As a result of the formation of a more robust metallogel network in MG3 system, vanadium ions and water molecules are arranged in a more orderly manner inside of the DMF, BTC, and adenine molecules' network.

To study the dynamic properties of the metallogel, five V<sup>III</sup> ions were randomly marked and their 3D trajectories (under ambient conditions in the last 4 ns of simulation time) were studied to obtain the best gelation conditions (Fig. 4). As shown in Fig. 4 the obtained results show that by increasing the DMF/H<sub>2</sub>O solvent ratio, the DMF molecules aggregate more effectively around the metallic ions. As a result, the vanadium ions are entrapped by their neighboring DMF, BTC, and adenine

molecules by increasing the DMF/H<sub>2</sub>O solvent ratio. This ensures that in the MG3, the self-assembly of the components is not disturbed over the time and the moving patterns of vanadium ions within the structure are similar to each other (Fig. 4c). Interestingly, the similar translating moving pattern of metal ions in the MG3 system, demonstrates a relatively more ordered and robust metallogel network formation due to the robust potency of DMF molecules (Fig. 4). It was previously demonstrated in Fig. 2a that increasing the DMF/H<sub>2</sub>O solvent ratio results in forming a slightly more ordered arrangement of the DMF molecules around metallic ions. For more investigations, V<sup>III</sup> ions, are selected and their 2D trajectories with highlighted curves are tracked in the XY plane (Fig. S2†).

After evaluating the significant role of the self-assembly between metallic ion and the other components in the formation of metallogel, Voronoi tessellation demonstrates the proper representation of the evolution of this self-assembly. In the next step, the dynamic properties of the VGel were assessed

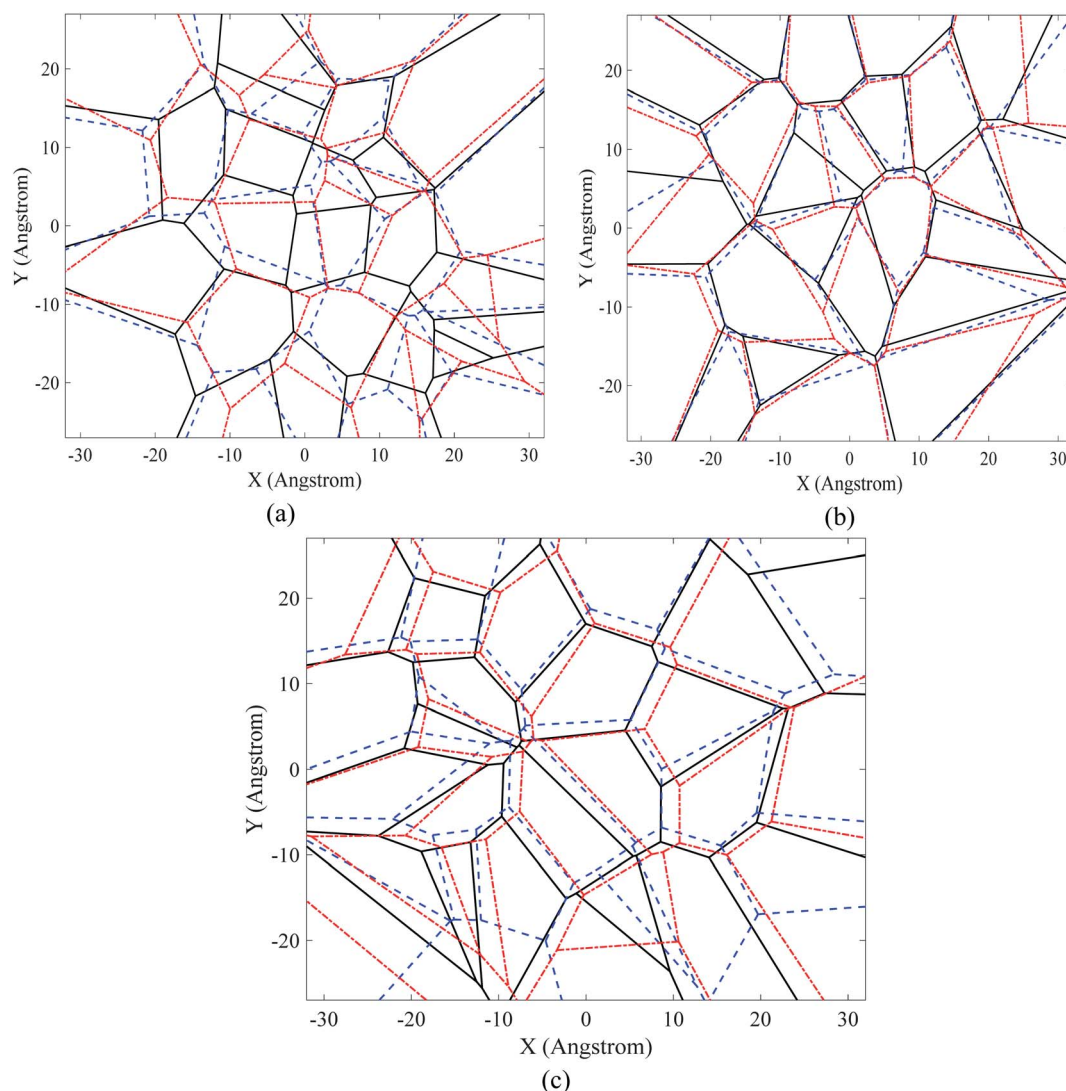


Fig. 5 The configuration of Voronoi tessellation for simulated systems at room temperature: (a) MG1, (b) MG2, and (c) MG3 (the configurations in 44.8, 44.9 and 45 ns are indicated in black, blue and red respectively).

using Voronoi tessellation. In the Voronoi tessellation, each vanadium coordinate (by projection on the  $XY$  plane) is depicted as the center of a Voronoi cell with metal ion core and specified boundary. The Voronoi cells for half of the selected vanadium ions are simulated for each of the MG1, MG2, and MG3 systems at 44.8, 44.9, and 45 ns (Fig. 5).

As shown in Fig. 5, when the metallogel is not formed firmly in the MG1 system, the new Voronoi networks are constantly disintegrated and altered over time, and undergoes significant changes in its geometrical shape. As displayed in Fig. 5, in the MG3 system, with a more stable gel, after gel formation, the geometrical shape of the Voronoi cells inside the box does not change remarkably over the time, but the whole set experiences a limited transfer displacement over the time. In comparison with the Voronoi evolution in MG1, by increasing the stability of the formed gel in the MG2 and MG3 cases, the Voronoi cell tests changed to more stable networks.

Calculating the mean standard deviation (SD) of each cell's area over time is a leading method for quantitative investigations of Voronoi cells. As a result, SD of the MG1 system calculated  $11.3933 \text{ \AA}^2$ , while for the MG2 and MG3 systems  $6.0556$  and  $4.2319 \text{ \AA}^2$ , respectively. The time evolution of Voronoi tessellation for the simulated systems is presented in the ESI Video (see ESI 2†).

**3.2.1. Interaction energies.** To understand the self-assembly mechanism of the metallogel components in the nanoscale, the non-covalent (van der Waals and electrostatic) interactions between  $V^{III}$  and other component molecules, were investigated through MD simulation (Table 1). In all simulated systems (MG1, MG2, and MG3),  $V^{III}$  ions did not aggregate with gelator molecules ( $V^{III}$ :BTC and  $V^{III}$ :Ade), which are indicated by relatively insignificant non-covalent energies. In contrast, the calculated energies between  $V^{III}$  ions and solvent molecules ( $V^{III}$ : $H_2O$  and  $V^{III}$ :DMF), were considerable. In more detail by increasing the DMF participation in the gel network from MG1 to MG2 and MG3 the calculated energies for  $V^{III}$ :DMF unlike  $V^{III}$ : $H_2O$  increased in a parallel manner. The negative charge and value of all the calculated electrostatic energies for  $V^{III}$ -solvents interactions with the vdW interactions, represented their attractive type and prominent role in the gelation process, respectively. Based on the experimental section, we could conclude that after the reduction of  $V^{IV}O^{2+}$  complexes to  $V^{III}$  ions, strong electrostatic potential energies have presided over  $V^{III}$  and  $H_2O$  molecular aggregations formed almost

immediately. However, by increasing the DMF/ $H_2O$  ratio, from MG1 to MG2 and MG3, the movement of  $V^{III}$  ions is more restricted which leads to the gel formation. It is noteworthy that this result is in good agreement with the experimental studies by Szejgis *et al.* that by increasing the organic solvent content, the size of the solvation shell increased and the mobility of the cation was reduced.<sup>71</sup>

Time evolution of the vdW and electrostatic interactions between the gel contents in the MG1, MG2, and MG3 systems are investigated in detail (Fig. S3 and S4†). To specify the gelator molecules' (BTC and Ade) structural alterations, we needed a numerical insight into their non-covalent interactions by studying their  $\pi$ - $\pi$  stacking interactions (Table 2). On the other hand, it is worth mentioning that  $\pi$ - $\pi$  stacking and  $\pi$ -cation interactions is recognized as stable and strong as hydrogen bonds and salt bridges.<sup>35–39</sup>

In all MG1 to MG3 simulated systems, small aggregates of gelator molecules were preferentially organized in a parallel fashion, around the solvated  $V^{III}$  ions and the calculated centroid-centroid distances between adjacent gelator molecules were in better agreement with previous reports in the MG3 simulation (Table 2).<sup>72,73</sup> We studied the RDF of  $V^{III}$  cations concerning the BTC and Ade molecules, confirming the gelator molecules aggregation around the  $V^{III}$  cations (Fig. S5†).

In Fig. 6, the snapshot of the  $\pi$ - $\pi$  stacked orientation of the BTC with BTC and Ade with BTC molecules is illustrated in all simulated systems. According to previous experimental studies, BTC molecules aggregate by increasing the DMF/ $H_2O$  ratio, from MG1 to MG2 and MG3, the solubility of the BTC is increased<sup>74</sup> and as a result, the length of the  $\pi$ - $\pi$  stacked BTC fibers is decreased to only 2 or 3 molecules. As proved by earlier

**Table 2** The centroid-centroid distance between the benzene ring of two adjacent BTC and adenine-BTC molecules in MG1 and MG3 systems at ambient conditions

	MG1	MG3
Centroid-centroid distance between two hexagonal ring ( $\text{\AA}$ )		
BTC-BTC	$3.9623 \pm 0.2974$	$3.8692 \pm 0.2477$
Adenine-BTC	$3.9220 \pm 0.3294$	$3.7161 \pm 0.2208$

**Table 1** The vdW and electrostatic interaction energies between  $V^{III}$  ions and other components in MG1, MG2 and MG3 systems under ambient conditions

	MG1		MG2		MG3	
Interaction energy of vanadium &	vdW ( $\text{kcal mol}^{-1}$ )	Electrostatic ( $\text{kcal mol}^{-1}$ )	vdW ( $\text{kcal mol}^{-1}$ )	Electrostatic ( $\text{kcal mol}^{-1}$ )	vdW ( $\text{kcal mol}^{-1}$ )	Electrostatic ( $\text{kcal mol}^{-1}$ )
Water	$2639.74 \pm 69.34$	$-42070.08 \pm 1008.49$	$2555.91 \pm 62.11$	$-37829.67 \pm 801.03$	$2259.94 \pm 61.85$	$-30240.75 \pm 666.88$
DMF	$38.94 \pm 10.93$	$-2588.74 \pm 242.39$	$118.98 \pm 15.64$	$-5821.16 \pm 344.60$	$411.27 \pm 34.91$	$-12824.91 \pm 597.58$
Adenine	$-1.68 \pm 0.24$	$27.63 \pm 44.97$	$-1.82 \pm 0.26$	$16.81 \pm 44.96$	$-1.90 \pm 0.26$	$3.80 \pm 41.51$
$H_3\text{BTC}$	$-1.59 \pm 0.35$	$-215.77 \pm 54.99$	$-1.73 \pm 0.25$	$-210.06 \pm 53.20$	$-1.84 \pm 0.46$	$-202.38 \pm 47.89$





Fig. 6 Top view snapshot of the  $\pi$ - $\pi$  stacked orientations' interactions between (a) two adjacent BTC and (b) adenine-BTC molecules in MG1, MG2, and MG3 systems.

studies, the gelator molecules, BTC and adenine, can form  $\pi$ - $\pi$  stacked fibers.<sup>72</sup> However, as demonstrated in Fig. S6 and S7,<sup>†</sup> by increasing the DMF/H<sub>2</sub>O ratio, from MG1 to MG2 and MG3, the length of the  $\pi$ - $\pi$  stacked fibers is decreased to only 2 or 3 molecules.

**3.2.2. Mechanical behavior under shear stress loading.** We also employed the steering MD simulation technique to investigate the mechanical properties and rheological behavior of our metallogel in shear loading. All the MG1, MG2, and MG3 systems were simulated and exposed to shear stress with a pulling velocity of  $1 \text{ \AA ns}^{-1}$  for 40 ns. Afterwards, the initial and final configurations, as well as the time evolutions for each case, were depicted in Fig. S8<sup>†</sup> and 7, respectively.

As demonstrated in Fig. 7 the required shear stress for deformation of simulated networks was different for each case, deviated from each other after 15 ns, and increased from MG1 to MG3 through the gel formation.<sup>75–79</sup> This indicates an increase in the shear strength of the VGel in the MG3 system, in which the gel components has a more robust self-assembly. Increasing the DMF/H<sub>2</sub>O solvent ratio in the system leads to more ordered structure that ultimately increases the integrity of the gel. van der Waals and electrostatic interaction energies are also in agreement with the above results. A set of these conditions makes the metallogel more resistant during applying

shear stress. This is in proper agreement with the observations made about the structure of the systems in Section 3.3.

In accordance with previous research studies, throughout the gelation process, mechanical properties such as the rigidity of metallogels and hydrogels are increased due to gelation.<sup>75–78</sup> The enhanced shear strength of the MG3 metallogel reinforces the assumption that this *structure* is likely to be more resistant to deformation. This assumption can be assessed in subsequent computational studies by calculating the viscosity of the metallogel networks.

### 3.3. Characterization and solvent stimuli-response of the VGel

The resultant metallogel (VGel) and its reactants were investigated with Fourier Transform-IR spectroscopy (FT-IR), SEM and the compartment vanadium ions were characterized with UV-visible absorption spectrum [Fig. S9–S12<sup>†</sup>]. The rheological and self-healing behavior of the gel was also studied [Fig. S13–S15 in the ESI<sup>†</sup>].

Moreover, since the VGel was prepared by a simple solvothermal reaction in the H<sub>2</sub>O/DMF solvent mixture it shows great stability in the H<sub>2</sub>O/DMF mixture. We specified that VGel interestingly displays a robust solvent dependent stability and appropriately a solvent stimuli-response property. To verify the stimuli-response, the gel network stability and color change of the VGel samples, in the presence of distilled water, DMF, ethanol ( $\geq 99.5\%$ ), methanol (99.8%), 1-propanol, 1-butanol, phenol, benzyl alcohol, dichloromethane, dimethyl sulfoxide, chloroform, and cyclohexane, were monitored by the naked eye. As shown in Fig. S12,<sup>†</sup> in the presence of ethanol the gel network and color of the VGel is destructed and changed from dark green to yellow after 30 seconds and 3 minutes, respectively, while in the case of methanol the mentioned times were changed to 5 minutes and 30 minutes, and in the presence of water, the network integrity and seaweed green color of the VGel network remained stable and showed no marked visible changes even after a couple of months. From these observations, we concluded that the fascinating variable colors of

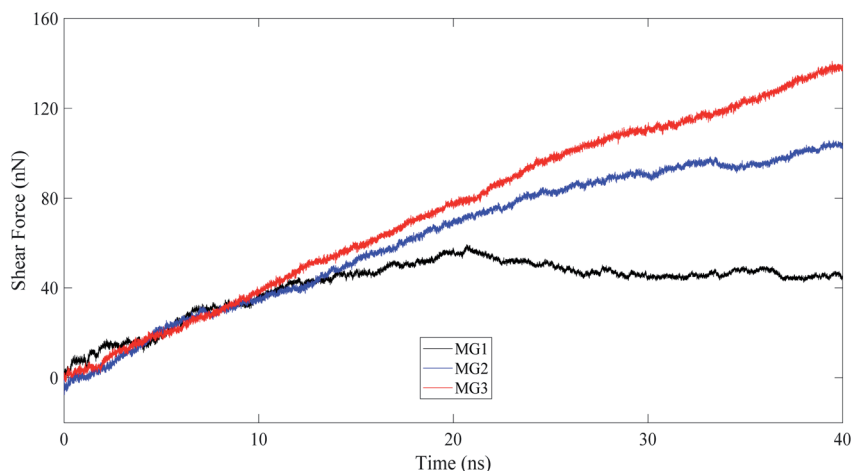


Fig. 7 Time evolution of shear force loading in the simulated systems at room temperature.

different vanadium ions made the VGel suitable for redox-responsive properties. These unique properties of VGel, lead us to develop a fast and easy visualization assay for measuring alcohol content and detecting methanol-spiked liquor.

### 3.4. Alcohol content visualization and quantification

Based on previous reports (Fig. S10†),<sup>80,81</sup> and MD simulations (Section 3.1), we concluded that redox-active  $V^{III}$  ions were readily entrapped into the VGel. The solvent stimuli-responsive property of VGel as described above (Section 3.3), along with the  $V^{III}/V^V$  redox chemistry brings out the basis of our proposed simple visualization assay. As shown in Fig. 8a and b, the addition of ethanol/water mixtures with different ratios (0–60% (v/v), 1 ml) into the 1.37 g samples of VGel, that were prepared with a 3 minute mild vortex, the color of the VGel samples gradually turns from seaweed green to yellow and simultaneously decreases the absorbance intensity.

These results represent an increase in the rate of  $V^{III}/V^V$  redox reaction as a function of increased ethanol concentration, proving the alcohol content of the liquor could be easily visualized by the naked eye through the color change of the VGel from dark green to yellow. Moreover, to develop an easy and fast technical method for quantification of alcohol content, we employed the solvent stimuli-response property along with UV-visible spectroscopy. For this purpose, 1.37 g samples of VGel were immersed in the different ethanol/water ratio mixtures for 150 seconds (2.5 minutes). In this case, the intensity of the absorption peak at 581 nm could be used as a signal for alcohol content quantification (Fig. 8b). As demonstrated in Fig. 8c the intensity of the absorption increases linearly with the enhancement of the alcohol content from 0% to 60% ( $y = -0.0153x + 1.3682$ ,  $R = 0.9952$ ). This result validates our

employed method for visualization and quantification of alcohol content.

Fig. 9a and c show typical UV-vis spectra of VGel decolorization at given time intervals for EtOH and MeOH, respectively. For both alcohols, the intensity of maximum absorption wavelengths gradually decreased by increasing the time. After 2.5 and 30 min, for EtOH and MeOH respectively, peaks at 581 nm vanish completely suggesting VGel complete decomposition with different rates. The rate constants  $k$  for EtOH and MeOH were determined by linear plots of  $A_t/A_0$  and  $\ln(A_t/A_0)$  over time match by zero- and pseudo-first-order reaction equations, respectively (Fig. 9b and d).

### 3.5. Differentiation of methanol-spiked liquor

To test our hypothesis, we attempted to analyze methanol in the headspace of counterfeit beverages, the detector not only was able to differentiate between methanol and ethanol molecules with high chemical and physical similarity, but also was able to differentiate methanol in the presence of very high ethanol concentrations. For this purpose, the stimuli-response of VGel samples (1.37 g) that were exposed to methanol for 150 seconds, in the range of 0.4–12.4% with an interfering ethanol concentration of 40%, were investigated. As shown in Fig. 10 the absorbance intensity has a strong linear dependency with methanol concentration and is represented with the equation  $y = 0.084x + 0.5964$  and  $R^2 = 0.9918$ . As described above this behavior was presumably illustrated by the redox reaction of  $V^{III}/V^V$  in the presence of ethanol. The presence of methanol, also in trace amounts increases the stability of the VGel, resulting in slower color change by decreasing the rate of  $V^{III}/V^V$  redox reaction. The limit of detection (LOD) was calculated according to the  $3\sigma/s$  criterion, where  $\sigma$  is the standard

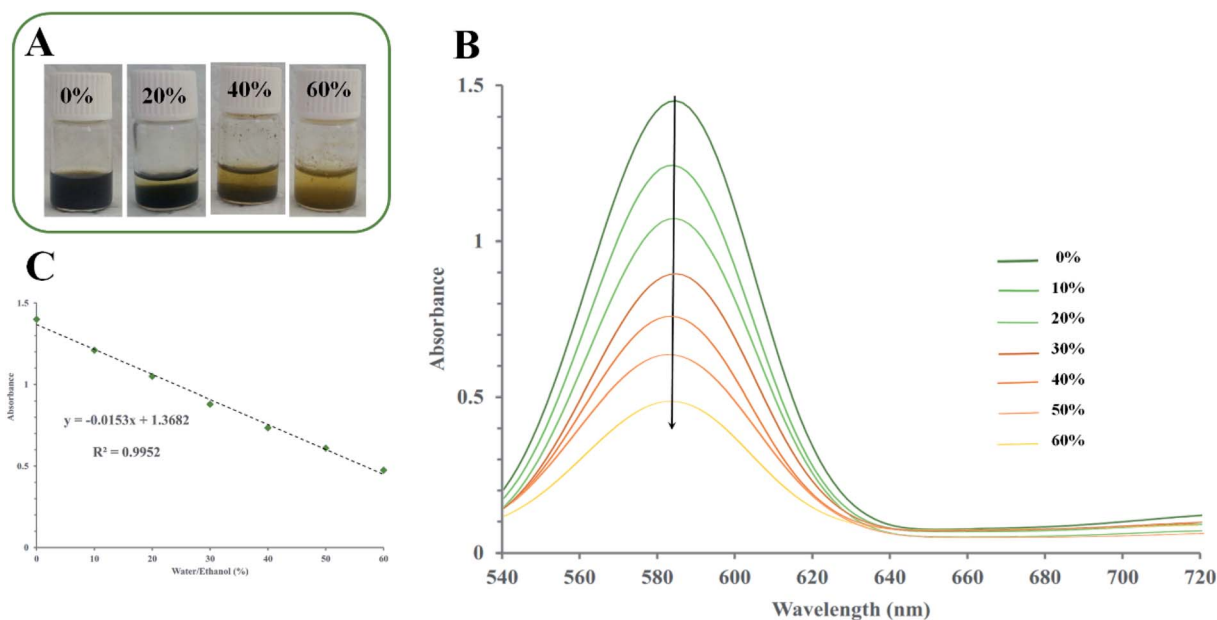


Fig. 8 (A) Color change photographs of VGel pieces (1.37 g) resulted from the addition of 1 ml of ethanol/water mixtures (vol% 0, 20, 40, and 60), (B) UV-visible absorption of VGel pieces (1.37 g) resulted from the addition of 1 ml of ethanol/water mixtures (vol% 0, 10, 20, 30, 40, 50 and 60) at 581 nm. (C) Beer-Lambert linear relationship of absorption intensity at 581 nm and ethanol concentrations of described mixtures in (C).



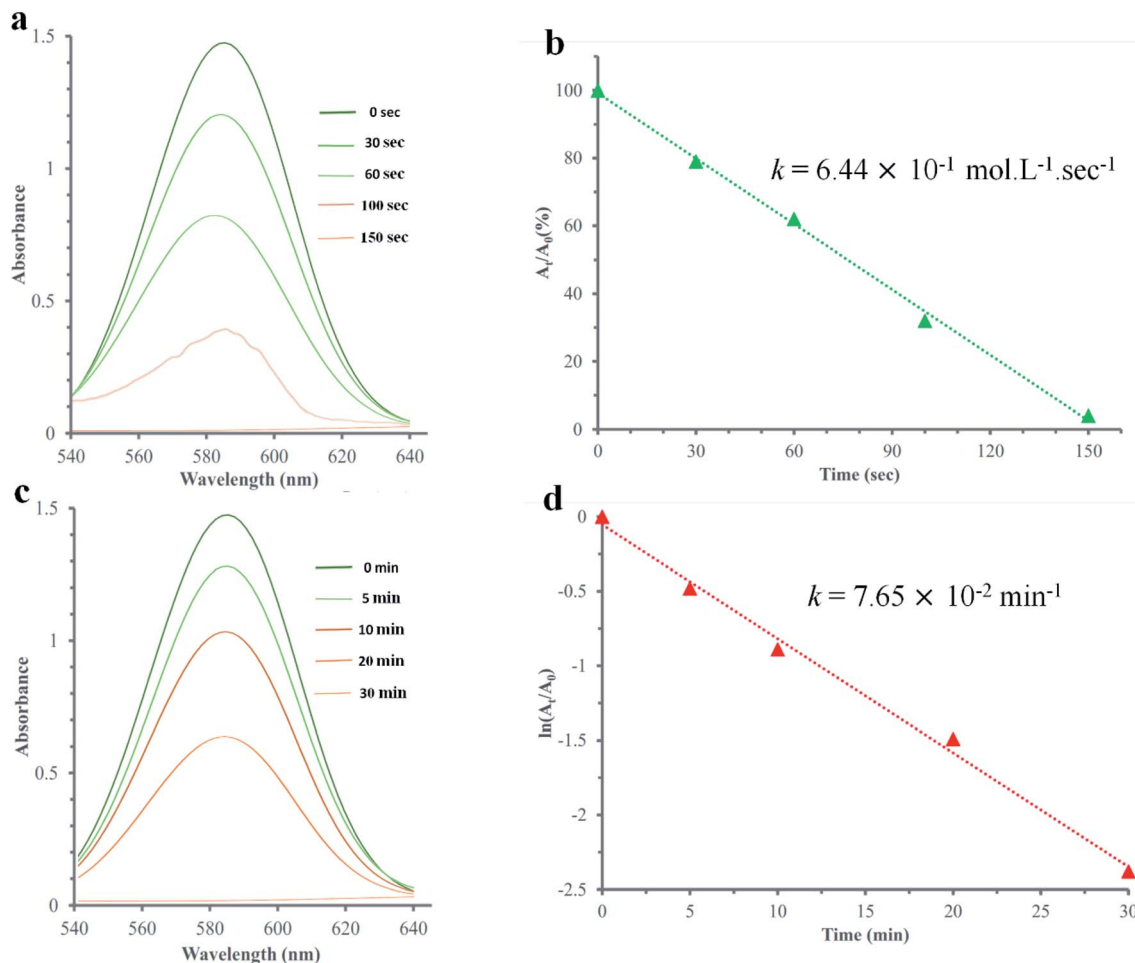


Fig. 9 (a and c) Time-dependent UV-vis spectra of the VGel in the presence of ethanol and methanol, respectively; (b and d) reaction rate constant  $k$  estimated by the slope of  $A_t/A_0$  and  $\ln(A_t/A_0)$  vs. reaction time.

deviation (SD) for each methanol with  $n = 5$  measurements and  $s$  is the slope. The calculated LOD for methanol percent detection was calculated 6% (v/v) of methanol in 40% (v/v) of ethanol.

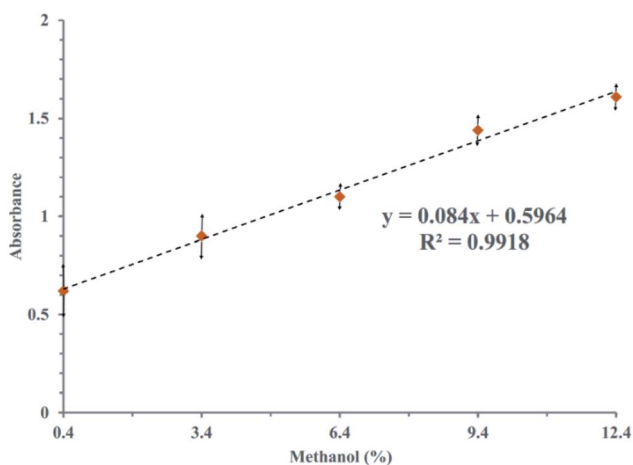


Fig. 10 Beer-Lambert linear relationship of absorption of VGel pieces (1.37 g) resulted from the addition of 1 ml of methanol (vol% 0.4, 3.4, 6.4, 9.4, 12.4 in 40% volume ethanol) for 5 times at 581 nm.

These results propose a great potential for the on-spot detection of counterfeit beverages.

Overall, the great solvent stimuli-responsive properties of VGel enable us to declare a reasonable promise for introducing a novel metallo gel for visualizing alcohol content and counterfeit liquor, as a technically simple and cheap method.

## 4. Conclusion

In conclusion, using a simple crystal engineering trick we were able to introduce the vanadium metal ion into the trimesic acid and adenine organogel and prepare a solvent stimuli-responsive metallo gel (VGel). In the simulation section of this work, the structural and dynamic properties, as well as the mechanical behavior of the metallo gel were investigated using molecular dynamics simulations. The radial distribution functions and the position of vanadium atoms results in three MG1, MG2, and MG3 systems showing that by increasing DMF/H<sub>2</sub>O solvent ratio the metallo gel network forms more effectively. For a better understanding of mechanical-behavior of the gel network, a shearing force with a constant pulling velocity was individually applied to the systems. Numerical results indicate a higher

shear force and almost elastic behavior with significant shear rigidity in MG3 compared to the MG1 and MG2 cases. As expected, by spatial coordinates and Voronoi tessellation assessments of the vanadium ions after gelation in the MG3 system, the network did not reveal particular alterations over the simulation time.

By exploiting the unique properties of VGel, including its excellent water stability and solvent stimuli-responsive specification, a technically easy and fast visualization method for on-spot recognition of alcohol content and detection of methanol-spiked liquor have been successfully developed. The special and noteworthy superiorities of our demonstrated essay over ordinary methods are its low cost, green chemical components, rapid sensing feature, and simplicity of the operation and instrumentation. These superiorities signify the suitability of this visualization essay as a promising method for alcohol content sensing and methanol-spiked liquor detection.

## Author contributions

Methodology, formal analysis, synthesis, investigations and writing the original draft, S. S.; review, editing and project administration, J. S.; MD simulations administration, M. F.; MD simulations, M. E., and V. F. N.; writing the original MD simulations section draft M. F., M. E., and V. F. N.; supervision, J. S. and M. F.; all authors have read and agreed to the published version of the manuscript.

## Conflicts of interest

There are no conflicts to declare.

## Acknowledgements

Funding for this research was provided by the University of Tehran.

## References

- 1 J. A. Kruse, Methanol poisoning, *Intensive Care Med.*, 1992, **18**, 391–397, DOI: 10.1007/BF01694340.
- 2 D. G. Barceloux, G. R. Bond, E. P. Krenzelok, H. Cooper and J. A. Vale, American Academy of Clinical Toxicology Practice Guidelines on the Treatment of Methanol Poisoning, *Clin. Toxicol.*, 2002, **40**, 415–446, DOI: 10.1081/CLT-120006745.
- 3 K. E. Hovda, O. H. Hunderi, A. B. Tafjord, O. Dunlop, N. Rudberg and D. Jacobsen, Methanol outbreak in Norway 2002–2004: epidemiology, clinical features and prognostic signs, *Ann. Intern. Med.*, 2005, **258**, 181–190, DOI: 10.1111/j.1365-2796.2005.01521.x.
- 4 I. L. Bennett, F. H. Cary, G. L. Mitchell and M. N. Cooper, Acute methyl alcohol poisoning: a review based on experiences in an outbreak of 323 cases, *Medicine*, 1953, **32**, 431–463, DOI: 10.1097/00005792-195312000-00002.
- 5 P. Levy, A. Hexdall, P. Gordon, C. Boeriu, M. Heller and L. Nelson, Methanol contamination of Romanian home-distilled alcohol, *Clin. Toxicol.*, 2003, **41**, 23–28, DOI: 10.1081/clt-120018267.
- 6 A. J. Paine and A. D. Dayan, Defining a tolerable concentration of methanol in alcoholic drinks, *Hum. Exp. Toxicol.*, 2001, **20**, 563–568, DOI: 10.1191/096032701718620864.
- 7 P. Tipparat, S. Lapanantnoppakhun, J. Jakmunee and K. Grudpan, Determination of ethanol in liquor by near-infrared spectrophotometry with flow injection, *Talanta*, 2001, **53**, 1199–1204, DOI: 10.1016/S0039-9140(00)00610-X.
- 8 A. Yildirim, F. E. Ozturk and M. Bayindir, Smelling in chemically complex environments: an optofluidic Bragg fiber array for differentiation of methanol adulterated beverages, *Anal. Chem.*, 2013, **85**, 6384–6391, DOI: 10.1021/ac4008013.
- 9 L. S. Mendes, F. C. Oliveira, P. A. Suarez and J. C. Rubim, Determination of ethanol in fuel ethanol and beverages by Fourier transform (FT)-near infrared and FT-Raman spectrometries, *Anal. Chim. Acta*, 2003, **493**, 219–231, DOI: 10.1016/S0003-2670(03)00870-5.
- 10 A. Nordon, A. Mills, R. T. Burn, F. M. Cusick and D. Littlejohn, Comparison of non-invasive NIR and Raman spectrometries for determination of alcohol content of spirits, *Anal. Chim. Acta*, 2005, **548**, 148–158, DOI: 10.1016/j.aca.2005.05.067.
- 11 I. H. Boyaci, H. E. Genis, B. Guven, U. Tamer and N. Alper, A novel method for quantification of ethanol and methanol in distilled alcoholic beverages using Raman spectroscopy, *J. Raman Spectrosc.*, 2012, **43**, 1171–1176, DOI: 10.1002/jrs.3159.
- 12 A. Mentana, C. Palermo, D. Nardiello, M. Quinto and D. Centonze, Simultaneous and accurate real-time monitoring of glucose and ethanol in alcoholic drinks, must, and biomass by a dual-amperometric biosensor, *J. Agric. Food Chem.*, 2013, **61**, 61–68, DOI: 10.1021/jf3031474.
- 13 M. Hnaïen, F. Lagarde and N. Jaffrezic-Renault, A rapid and sensitive alcohol oxidase/catalase conductometric biosensor for alcohol determination, *Talanta*, 2010, **81**, 222–227, DOI: 10.1016/j.talanta.2009.11.061.
- 14 K. Svensson, L. Bülow, D. Kriz and M. Krook, Investigation and evaluation of a method for determination of ethanol with the SIRE® Biosensor P100, using alcohol dehydrogenase as recognition element, *Biosens. Bioelectron.*, 2005, **21**, 705–711, DOI: 10.1016/j.bios.2005.01.001.
- 15 J. Van den Broek, S. Abegg, S. E. Pratsinis and A. T. Güntner, Highly selective detection of methanol over ethanol by a handheld gas sensor, *Nat. Commun.*, 2019, **10**, 1–8, DOI: 10.1038/s41467-019-12223-4.
- 16 C. A. Weatherly, R. M. Woods and D. W. Armstrong, Rapid analysis of ethanol and water in commercial products using ionic liquid capillary gas chromatography with thermal conductivity detection and/or barrier discharge ionization detection, *J. Agric. Food Chem.*, 2014, **62**, 1832–1838, DOI: 10.1021/jf4050167.
- 17 A. Terol, E. Paredes, S. E. Maestre, S. Prats and J. L. Todolí, Alcohol and metal determination in alcoholic beverages



- through high-temperature liquid-chromatography coupled to an inductively coupled plasma atomic emission spectrometer, *J. Chromatogr. A*, 2011, **1218**, 3439–3446, DOI: 10.1016/j.chroma.2011.03.060.
- 18 M. O. Fogwill and K. B. Thurbide, Chromatography using a water stationary phase and a carbon dioxide mobile phase, *Anal. Chem.*, 2010, **82**, 10060–10067, DOI: 10.1021/ac1018793.
  - 19 H. Li, X. S. Chai, Y. Deng, H. Zhan and S. Fu, Rapid determination of ethanol in fermentation liquor by full evaporation headspace gas chromatography, *J. Chromatogr. A*, 2009, **1216**, 169–172, DOI: 10.1016/j.chroma.2008.11.024.
  - 20 A. A. Marti, S. Jockusch, N. Stevens, J. Ju and N. J. Turro, Fluorescent hybridization probes for sensitive and selective DNA and RNA detection, *Acc. Chem. Res.*, 2007, **40**, 402–409, DOI: 10.1021/ar600013q.
  - 21 M. L. Wang, J. T. Wang and Y. M. Choong, A rapid and accurate method for determination of methanol in alcoholic beverage by direct injection capillary gas chromatography, *J. Food. Compos. Anal.*, 2004, **17**, 187–196, DOI: 10.1016/j.jfca.2003.08.006.
  - 22 G. Cabello, K. C. Nwoko, J. F. Marco, M. Sánchez-Arenillas, A. M. Méndez-Torres, J. Feldmann and T. A. Smith, Cu@Au self-assembled nanoparticles as SERS-active substrates for (bio) molecular sensing, *J. Alloys Compd.*, 2019, **791**, 184–192, DOI: 10.1016/j.jallcom.2019.03.279.
  - 23 S. Fateixa, H. I. Nogueira and T. Trindade, Hybrid nanostructures for SERS: materials development and chemical detection, *Phys. Chem. Chem. Phys.*, 2015, **17**, 21046–21071, DOI: 10.1039/C5CP01032B.
  - 24 G. B. Demirel, B. Daglar and M. Bayindir, Extremely fast and highly selective detection of nitroaromatic explosive vapours using fluorescent polymer thin films, *Chem. Commun.*, 2013, **49**, 6140–6142, DOI: 10.1039/C3CC43202E.
  - 25 R. Freeman and I. Willner, Optical molecular sensing with semiconductor quantum dots (QDs), *Chem. Soc. Rev.*, 2012, **41**, 4067–4085, DOI: 10.1039/C2CS15357B.
  - 26 M. E. Germain and M. J. Knapp, Optical explosives detection: from color changes to fluorescence turn-on, *Chem. Soc. Rev.*, 2009, **38**, 2543–2555, DOI: 10.1039/B809631G.
  - 27 Y. Zhang, S. Yuan, G. Day, X. Wang, X. Yang and H. C. Zhou, Luminescent sensors based on metal-organic frameworks, *Coord. Chem. Rev.*, 2018, **354**, 28–45, DOI: 10.1016/j.ccr.2017.06.007.
  - 28 P. Kumar, A. Deep and K. H. Kim, Metal organic frameworks for sensing applications, *TrAC, Trends Anal. Chem.*, 2015, **73**, 39–53, DOI: 10.1016/j.trac.2015.04.009.
  - 29 Y. Cui, B. Chen and G. Qian, Lanthanide metal-organic frameworks for luminescent sensing and light-emitting applications, *Coord. Chem. Rev.*, 2014, **273**, 76–86, DOI: 10.1016/j.ccr.2013.10.023.
  - 30 K. Liu, T. Liu, X. Chen, X. Sun and Y. Fang, Fluorescent films based on molecular-gel networks and their sensing performances, *ACS Appl. Mater. Interfaces*, 2013, **5**, 9830–9836, DOI: 10.1021/am4030774.
  - 31 J. Zhang, Y. Hu and Y. Li, Metal–Organic Gels, *Gel Chemistry*, Springer, Singapore, 2018, vol. 96, pp. 61–118.
  - 32 P. Dastidar, S. Ganguly and K. Sarkar, Metallogels from coordination complexes, organometallic, and coordination polymers, *Chem.-Asian J.*, 2016, **11**, 2484–2498, DOI: 10.1002/asia.201600814.
  - 33 P. Sutar and T. K. Maji, Coordination polymer gels: soft metal–organic supramolecular materials and versatile applications, *Chem. Commun.*, 2016, **52**, 8055–8074, DOI: 10.1039/C6CC01955B.
  - 34 H. Lee, S. H. Jung, W. S. Han, J. H. Moon, S. Kang, J. Y. Lee and S. Shinkai, A Chromo-Fluorogenic Tetrazole-Based CoBr<sub>2</sub> Coordination Polymer Gel as a Highly Sensitive and Selective Chemosensor for Volatile Gases Containing Chloride, *Chem.-Eur. J.*, 2011, **17**, 2823–2827, DOI: 10.1002/chem.201003279.
  - 35 L. Li, N. Zhou, H. Kong and X. He, Controlling the supramolecular polymerization and metallogel formation of Pt(II) complexes *via* delicate tuning of non-covalent interactions, *Polym. Chem.*, 2019, **10**, 5465–5472, DOI: 10.1039/C9PY01299K.
  - 36 Q. Zhou, X. Dong, J. Yuan, B. Zhang, S. Lu, Q. Wang, Y. Liao, Y. Yang and H. Wang, Reversible redox switching of concurrent luminescence and visual color change based on lanthanide metallogel, *Langmuir*, 2019, **35**, 15344–15351, DOI: 10.1021/acs.langmuir.9b02828.
  - 37 Q. Lin, T. T. Lu, X. Zhu, B. Sun, Q. P. Yang, T. B. Wei and Y. M. Zhang, A novel supramolecular metallogel-based high-resolution anion sensor array, *Chem. Commun.*, 2015, **51**, 1635–1638, DOI: 10.1039/C4CC07814D.
  - 38 L. Zhang, H. Qi, Y. Wang, L. Yang, P. Yu and L. Mao, Effective visualization assay for alcohol content sensing and methanol differentiation with solvent stimuli-responsive supramolecular ionic materials, *Anal. Chem.*, 2014, **86**, 7280–7285, DOI: 10.1021/ac5014546.
  - 39 S. Sarkar, S. Dutta, S. Chakrabarti, P. Bairi and T. Pal, Redox-switchable copper(I) metallogel: a metal–organic material for selective and naked-eye sensing of picric acid, *ACS Appl. Mater. Interfaces*, 2014, **6**, 6308–6316, DOI: 10.1021/am501491u.
  - 40 M. A. Ramin, L. Latxague, K. R. Sindhu, O. Chassande and P. Barthélémy, Low molecular weight hydrogels derived from urea based-bolaamphiphiles as new injectable biomaterials, *Biomaterials*, 2017, **145**, 72–80, DOI: 10.1016/j.biomaterials.2017.08.034.
  - 41 D. K. Kumar and J. W. Steed, Supramolecular gel phase crystallization: orthogonal self-assembly under non-equilibrium conditions, *Chem. Soc. Rev.*, 2014, **43**, 2080–2088, DOI: 10.1039/C3CS60224A.
  - 42 X. Yu, L. Chen, M. Zhang and T. Yi, Low-molecular-mass gels responding to ultrasound and mechanical stress: towards self-healing materials, *Chem. Soc. Rev.*, 2014, **43**, 5346–5371, DOI: 10.1039/C4CS00066H.
  - 43 W. Fang, Y. Zhang, J. Wu, C. Liu, H. Zhu and T. Tu, Recent advances in supramolecular gels and catalysis, *Chem.-Asian J.*, 2018, **13**(7), 712–729, DOI: 10.1002/asia.201800017.
  - 44 A. Y. Y. Tam and V. W. W. Yam, Recent advances in metallogels, *Chem. Soc. Rev.*, 2013, **42**, 1540–1567, DOI: 10.1039/C2CS35354G.



- 45 T. Tu, W. Fang, X. Bao, X. Li and K. H. Dötz, Visual chiral recognition through enantioselective metallogel collapsing: synthesis, characterization, and application of platinum-steroid low-molecular-mass gelators, *Angew. Chem., Int. Ed. Engl.*, 2011, **50**, 6601–6605, DOI: 10.1002/anie.201100620.
- 46 J. W. Steed, Anion-tuned supramolecular gels: a natural evolution from urea supramolecular chemistry, *Chem. Soc. Rev.*, 2010, **39**, 3686–3699, DOI: 10.1039/B926219A.
- 47 S. I. Kawano, N. Fujita and S. Shinkai, A coordination gelator that shows a reversible chromatic change and sol–gel phase-transition behavior upon oxidative/reductive stimuli, *J. Am. Chem. Soc.*, 2004, **126**, 8592–8593, DOI: 10.1021/ja048943+.
- 48 W. Miao, L. Zhang, X. Wang, H. Cao, Q. Jin and M. Liu, A Dual-Functional Metallogel of Amphiphilic Copper(II) Quinolinol: Redox Responsiveness and Enantioselectivity, *Chem.–Eur. J.*, 2013, **19**, 3029–3036, DOI: 10.1002/chem.201203401.
- 49 Y. He, Z. Bian, C. Kang, Y. Cheng and L. Gao, Chiral binaphthylbisbipyridine-based copper(I) coordination polymer gels as supramolecular catalysts, *Chem. Commun.*, 2010, **46**, 3532–3534, DOI: 10.1039/B926936C.
- 50 J. Liu, P. He, J. Yan, X. Fang, J. Peng, K. Liu and Y. Fang, An organometallic super-gelator with multiple-stimulus responsive properties, *Adv. Mater.*, 2008, **20**, 2508–2511, DOI: 10.1002/adma.200703195.
- 51 M. G. Angelerou, P. W. Frederix, M. Wallace, B. Yang, A. Rodger, D. J. Adams and M. Zelzer, Supramolecular nucleoside-based gel: molecular dynamics simulation and characterization of its nanoarchitecture and self-assembly mechanism, *Langmuir*, 2018, **34**, 6912–6921, DOI: 10.1021/acs.langmuir.8b00646.
- 52 G. Dalkas, A. B. Matheson, H. Vass, A. Gromov, G. O. Lloyd, V. Koutsos, P. S. Clegg and S. R. Euston, Molecular interactions behind the self-assembly and microstructure of mixed sterol organogels, *Langmuir*, 2018, **34**, 8629–8638, DOI: 10.1021/acs.langmuir.8b01208.
- 53 A. S. Côté, A. N. Cormack and A. Tilocca, Reactive molecular dynamics: An effective tool for modelling the sol–gel synthesis of bioglasses, *J. Mater. Sci.*, 2017, **52**, 9006–9013, DOI: 10.1007/s10853-017-1009-6.
- 54 X. Jiang, C. Wang and Q. Han, Molecular dynamic simulation on the state of water in poly(vinyl alcohol) hydrogel, *Comput. Theor. Chem.*, 2017, **1102**, 15–21, DOI: 10.1016/j.comptc.2016.12.041.
- 55 J. C. Phillips, R. Braun, W. Wang, J. Gumbart, E. Tajkhorshid, E. Villa, C. Chipot, R. D. Skeel, L. Kale and K. Schulten, Scalable Molecular Dynamics with NAMD, *J. Comput. Chem.*, 2005, **26**, 1781–1802, DOI: 10.1002/jcc.20289.
- 56 R. B. Best, X. Zhu, J. Shim, P. E. M. Lopes, J. Mittal, M. Feig and A. D. MacKerell Jr, Optimization of the Additive CHARMM All-Atom Protein Force Field Targeting Improved Sampling of the Backbone  $\phi$ ,  $\psi$  and Side-Chain X1 and X2 Dihedral Angles, *J. Chem. Theory Comput.*, 2012, **8**, 3257–3273, DOI: 10.1021/ct300400x.
- 57 J. Huang, S. Rauscher, G. Nawrocki, T. Ran, M. Feig, B. L. de Groot, H. Grubmüller and A. D. MacKerell Jr, CHARMM36m: An Improved Force Field for Folded and Intrinsically Disordered Proteins, *Nat. Methods*, 2017, **14**, 71–73, DOI: 10.1038/nmeth.4067.
- 58 N. Zhang, B. Yang, J. Huo, W. Qi, X. Zhang, X. Ruan, J. Bao and G. He, Hydration Structures of Vanadium/Oxovanadium Cations in the Presence of Sulfuric Acid: A Molecular Dynamics Simulation Study, *Chem. Eng. Sci.*, 2019, **195**, 683–692, DOI: 10.1016/j.ces.2018.10.014.
- 59 E. Wernersson and P. Jungwirth, Effect of Water Polarizability on the Properties of Solutions of Polyvalent Ions: Simulations of Aqueous Sodium Sulfate with Different Force Fields, *J. Chem. Theory Comput.*, 2010, **6**, 3233–3240, DOI: 10.1021/ct100465g.
- 60 W. R. Cannon, B. M. Pettitt and J. A. McCammon, Sulfate Anion in Water: Model Structural, Thermodynamic, and Dynamic Properties, *J. Phys. Chem.*, 1994, **98**, 6225–6230, DOI: 10.1021/j100075a027.
- 61 W. L. Jorgensen, J. Chandrasekhar, J. D. Madura, R. W. Impey and M. L. Klein, Comparison of Simple Potential Functions for Simulating Liquid Water, *J. Chem. Phys.*, 1983, **79**, 926–935, DOI: 10.1063/1.445869.
- 62 T. Darden, D. York and L. Pedersen, Particle Mesh Ewald: An N-Log(N) Method for Ewald Sums in Large Systems, *J. Chem. Phys.*, 1993, **98**, 10089–10092, DOI: 10.1063/1.464397.
- 63 W. Humphrey, A. Dalke and K. Schulten, VMD: Visual Molecular Dynamics, *J. Mol. Graphics*, 1996, **14**, 33–38, DOI: 10.1016/0263-7855(96)00018-5.
- 64 G. M. Peters and J. T. Davis, Supramolecular gels made from nucleobase, nucleoside and nucleotide analogs, *Chem. Soc. Rev.*, 2016, **45**, 3188–3206, DOI: 10.1039/C6CS00183A.
- 65 X. Liu, Q. Zhang, Z. Gao, R. Hou and G. Gao, Bioinspired adhesive hydrogel driven by adenine and thymine, *ACS Appl. Mater. Interfaces*, 2017, **9**, 17645–17652, DOI: 10.1021/acsami.7b04832.
- 66 H. Kuang, H. He, Z. Zhang, Y. Qi, Z. Xie, X. Jing and Y. Huang, Injectable and biodegradable supramolecular hydrogels formed by nucleobase-terminated poly(ethylene oxide)s and  $\alpha$ -cyclodextrin, *J. Mater. Chem. B*, 2014, **2**, 659–667, DOI: 10.1039/C3TB21475C.
- 67 P. K. Sukul and S. Malik, Supramolecular hydrogels of adenine: Morphological, structural and rheological investigations, *Soft Matter*, 2011, **7**, 4234–4241, DOI: 10.1039/C1SM05055A.
- 68 M. Maresca, A. Derghal, C. Carravagna, S. Dudin and J. Fantini, Controlled aggregation of adenine by sugars: physicochemical studies, molecular modelling simulations of sugar–aromatic CH– $\pi$  stacking interactions, and biological significance, *Phys. Chem. Chem. Phys.*, 2008, **10**, 2792–2800, DOI: 10.1039/B802594K.
- 69 J. Lu, C. Hu, H. Liu, H. Gao and Y. Ju, Water-induced gel formation of an oleanic acid–adenine conjugate and the effects of uracil derivative on the gel stability, *Soft Matter*, 2012, **8**, 9576–9580, DOI: 10.1039/C2SM26085A.



- 70 Z. Zhang and M. J. Zaworotko, Template-directed synthesis of metal-organic materials, *Chem. Soc. Rev.*, 2014, **43**, 5444–5455, DOI: 10.1039/C4CS00075G.
- 71 A. Szejgis, A. Bald, J. Gregorowicz and M. Żurada, Conductance Studies in Mixtures of Water with DMF at 298.15 K. Part VI. Lithium and Sodium Nitrates, Sodium Perchlorate and Propionate, Potassium Picrate and Thiocyanate, and Limiting Ionic Conductance, *J. Mol. Liq.*, 1999, **79**, 123–136, DOI: 10.1016/S0167-7322(98)00107-X.
- 72 A. Tahli, Ü. Kőc, R. Elshaarawy, A. Kautz and C. Janiak, A Cadmium Anionic 1-D Coordination Polymer  $\{[\text{Cd}(\text{H}_2\text{O})_6][\text{Cd}_2(\text{Atr})_2(\mu_2\text{-Btc})_2(\text{H}_2\text{O})_4]\cdot 2\text{H}_2\text{O}\}_n$  within a 3-D Supramolecular Charge-Assisted Hydrogen-Bonded and  $\pi$ -Stacking Network, *Crystals*, 2016, **6**, 23, DOI: 10.3390/cryst6030023.
- 73 A. Gładysiak, T. N. Nguyen, J. A. R. Navarro, M. J. Rosseinsky and K. C. Stylianou, A Recyclable Metal–Organic Framework as a Dual Detector and Adsorbent for Ammonia, *Chem.–Eur. J.*, 2017, **23**, 13602–13606, DOI: 10.1002/chem.201703510.
- 74 D. Zhang and Q. Xu, Solubility of 1,3,5-Benzenetricarboxylic Acid in Different Solvents, *J. Chem. Eng. Data*, 2016, **61**, 1003–1006, DOI: 10.1021/acs.jced.5b00870.
- 75 Z. Shen, T. Wang and M. Liu, Tuning the Gelation Ability of Racemic Mixture by Melamine: Enhanced Mechanical Rigidity and Tunable Nanoscale Chirality, *Langmuir*, 2014, **30**, 10772–10778, DOI: 10.1021/la502799j.
- 76 T. Feldner, M. Häring, S. Saha, J. Esquena, R. Banerjee and D. Díaz Díaz, Supramolecular Metallogel That Imparts Self-Healing Properties to Other Gel Networks, *Chem. Mater.*, 2016, **28**, 3210–3217, DOI: 10.1021/acs.chemmater.6b01144.
- 77 L. Cai, J. Li, S. Quan, W. Feng, J. Yao, M. Yang and W. Li, Dextran-based Hydrogel with Enhanced Mechanical Performance *via* Covalent and Non-covalent Cross-linking Units Carrying Adipose-derived Stem Cells toward Vascularized Bone Tissue Engineering, *J. Biomed. Mater. Res., Part A*, 2019, **107**, 1120–1131, DOI: 10.1002/jbm.a.36580.
- 78 T. Suekama, *Engineering the Microstructure of Hydrogels to Achieve Enhanced Mechanical Properties*, Doctoral dissertation, University of Kansas, 2014.
- 79 Y. Qiu and K. Park, Superporous IPN Hydrogels Having Enhanced Mechanical Properties, *AAPS PharmSciTech*, 2003, **4**, 406–412, DOI: 10.1208/pt040451.
- 80 C. Choi, S. Kim, R. Kim, Y. Choi, S. Kim, H. Y. Jung and H. T. Kim, A review of vanadium electrolytes for vanadium redox flow batteries, *Renewable Sustainable Energy Rev.*, 2017, **69**, 263–274, DOI: 10.1016/j.rser.2016.11.188.
- 81 M. R. Maurya, B. Sarkar, F. Avecilla and I. Correia, Vanadium (IV and V) complexes of pyrazolone based ligands: Synthesis, structural characterization and catalytic applications, *Dalton Trans.*, 2016, **45**, 17343–17364, DOI: 10.1039/C6DT03425J.

